A hybrid functional calculation of Tm^{3+} defects in germanium (Ge)

E. Igumbor[a,b,*], W. E. Meyer[a,**]

[a] *Department of Physics, University of Pretoria, Pretoria 0002, South Africa.*
[b] *Department of Mathematics and Physical Sciences, Samuel Adegboyega University, Km 1 Ogwa/Ehor Rd, Ogwa Edo State Nigeria.*

Abstract

In this work we present *ab-initio* calculation results for the Tm^{3+} interstitial (Tm_i^{3+}), vacancy-interstitial complex (V_{Ge}-Tm_i^{3+}) and substitutional (Tm_{Ge}^{3+}) defects in germanium (Ge) as determined by the density functional theory (DFT) using the Heyd, Scuseria, and Ernzerhof (HSE06) hybrid functional. We calculated the formation energies and the charge state transition levels of different configurations. Our results show that the Tm^{3+} interstitial exists in the hexagonal configuration with low formation energy. The formation energies for V_{Ge}-Tm_i^{3+} and Tm_{Ge}^{3+} were as low as 0.84 eV. The most energetically favourable defects were the V_{Ge}-Tm_i^{3+} in the *axial* configuration and the Tm_{Ge}^{3+}. The Tm_{Ge}^{3+} and V_{Ge}-Tm_i^{3+} introduced a single acceptor $\epsilon(0/-1)$ charge state transition level that was positioned deep in the middle of the band gap. The majority of the levels induced by the defects under investigation, were either shallow donor or acceptor level lying close to the band gap

*Corresponding author
**Corresponding author
Email addresses: elgumuk@gmail.com (E. Igumbor), wmeyer@up.ac.za (W. E. Meyer)

Postprint submitted to Materials Science in Semiconductor Processing December 8, 2015

edges.

Keywords: Defects, formation energy, charge state

1. Introduction

The application of germanium (Ge) in semiconductor material technology is attracting attention due to its high carrier mobilities[1, 2, 3]. The use of Ge technology has been successful lately due to the understanding of the role that defects play in it. The role of defects in Ge is well understood from their formation energies and transition charge state levels in the band gap. Studies of electronic properties of elemental radiation induced defects in Ge are relatively scarce and this deficiency recently led towards investigative experimenting and theoretical modelling[4, 5, 6] of defects in Ge. Deep level transient spectroscopy (DLTS)[7, 8] and infrared absorption spectroscopy [9] studies have succeeded in identifying new radiation induced defects paired with impurities. Perturbed angular correlation spectroscopy (PACs) studies[10, 11] have led to important findings on the mobility and electrical activities of vacancies (V) and interstitials (I); and lately, these two defects have been investigated after introduction at low temperature by in situ DLTS [7, 8]. Studies of *self*-, *di*- interstitials, vacancies and substitution related defects in Ge have attracted interest in the past decades [12]. Despite the effort made so far in identifying different defects in Ge, there is still more to be accomplished. The rare earth (RE) elements are known to have a partially filled inner *4f* shell which gives rise to sharp transitions that are largely insensitive to the crystal host and temperature variations [13, 14, 15]. RE element related defects such as Tm doping of ZnO[16], and other ma-

terials have been reported[17, 18, 19, 20, 21]. Thulium ions (Tm^{3+}) doped materials have been used to generate blue laser emission through non-linear up-conversion of radiation from the infrared to the visible range[17, 18, 22]. Recently optical properties of Tm doped materials were studied and EL has been observed from these materials [16, 23, 19]. Light emission has been attributed to thulium and erbium defects in material [13, 14, 15]. Previous studies of RE implanted Si showed sharp emission peaks that were attributed to Tm^{3+} [24]. While the Er was found in interstitial positions as well as in defect complexes [25], the cerium was found to act as an acceptor in a substitutional position in Si [26]. One would expect that Tm^{3+} interstitials or other related defects in Ge will create deep donor levels, however experimental studies of these defects are yet to be performed. In this work, using the hybrid functional of Heyd, Scuseria, and Ernzerhof (HSE06) [27], we have carried out a detailed density functional theory (DFT) calculation of the electronic properties of Tm^{3+} interstitial (Tm_i^{3+}) in the hexagonal (H) configuration, substitutional (Tm_{Ge}^{3+}) and vacancy-interstitial (V_{Ge}-Tm_i^{3+}) defects in Ge with a view to finding the most stable defect types from the formation energies of the various charge states. The charge state thermodynamic transition levels were also examined to determined the type of level induced in the band gap by Tm^{3+} defects. The rest of this paper has been organized as follows: in the next section, we present a description of the computational methodology. The results and discussion were presented in section 3. Finally, we present our concluding remarks in Section 4.

2. Computational details

We performed a DFT electronic structure calculation using the Vienna *ab-initio* Simulation Package (VASP) [28, 29]. The Projector-augmented wave (PAW) method, as implemented in the VASP code was used to separate the inert core electrons from the chemically active valence electrons [28, 30]. Calculations were carried out using the Heyd, Scuseria, and Ernzerhof (HSE06) [27] hybrid functional. In this approach, the short-range exchange potential is calculated by mixing a fraction of nonlocal Hartree-Fock exchange with the generalized gradient approximation (GGA) functional of Perdew, Burke, and Ernzerhof (PBE) [31]. In contrast to the *local density approximation* and the *generalized gradient approximation* that underestimate the band gap of the semiconductor [32, 33], the HSE06 functional gives an excellent description of the electronic band gap and charge state transition properties for a wide range of the defects in group-IV semiconductors [32, 34, 6]. For the past decades, the study and prediction of the electronic properties of materials with f orbital valence electrons was difficult due to the fact that the f orbital is highly localized. The highly localized f orbitals were previously treated using LDA+U and other methods [35, 36, 37, 38]. Recently, density functional theory using hybrid functionals has been successfully implemented, predicting the electronic and band gap properties of several materials with f orbital in the valence shell [35, 39]. Following the successful implementation of the hybrid functional, it became feasible for us to handle the f state in the valence shell of Tm^{3+}. For Ge, the $4s$ and $4p$ electrons in the outer shell were treated as valence electrons, while for Tm^{3+}, the $6s$, $5p$ and $4f$ orbitals were considered as valence electrons. For the bulk, geometric optimization

of Ge was performed on an 8-atom unit cell with an 8^3 Monkhorst-Pack [40] k-point Brillouin zone sampling scheme and cutoff energy of 600 eV. For the defects, we employed a 64 atom supercell using a 2^3 Monkhorst-Pack [40] k-point Brillouin zone sampling scheme, and we set the plane wave cutoff of the wave function expansion to 400 eV. We refined the geometry until the final change in the total energy was less than 10^{-5} eV and the forces were relaxed to below 0.001 eV/Å. In all the calculations, spin orbit coupling was taken into account. The formation energy (E^f) of defect is derived directly from total energies, allowing the calculation of equilibrium defect *concentrations* [41]. To calculate the defect formation and thermodynamic transition ($\epsilon(q/q')$) levels, we calculated the total energy E(d,q) for a supercell containing the optimized defect d in its charge state q. The defect formation energy $E^f(d,q)$ as a function of electron Fermi energy (ε_F) is given as [42, 43]

$$E^f(d,q) = E(d,q) - E(pure) + \sum_i (\triangle n)_i \mu_i + q[E_V + \varepsilon_F] + E^q_{cor}, \tag{1}$$

where $E(pure)$ is a supercell without a defect, $(\triangle n)_i$ is the difference in the number of constituent atoms of type i between the supercells, E_V is the valence band maximum (VBM) and μ_i represents the chemical potential of different constituent atoms. Errors in $E^f(d,q)$ due to finite-size effects within the supercell and inaccuracy underlying the approximation of the energy functional, were handled by including a correction term E^q_{cor} according to Freysoldt *et al* [42, 43]. The defect transition energy level $\epsilon(q/q')$ is the Fermi energy for which the formation energy of charge state q equals that of charge state q' and is given as [42]

$$\epsilon(q/q') = \frac{E^f(d,q;\ \varepsilon_F = 0) - E^f(d,q';\ \varepsilon_F = 0)}{q' - q} \tag{2}$$

The method proposed by Stephan *et al* [44] was used for the calculation of the ionization energy (I_A) related to the conduction band (CBM) and the electron affinity (E_A) related to valence band maximum (VBM). The pristine Kohn-Sham band gap of Ge was calculated to be 0.80 eV, which was higher than the experimental band gap at 0 K. For consistency, we employed the quasiparticle band gap [45, 44] calculation. From the calculated I_A and the E_A energies of 4.00 and 3.22 eV respectively, we obtained a Ge band gap of 0.78 eV, which is in agreement with the experimental band gap at 0 K reported by Morin *et al* [46]. The binding energies E_b which are defined as the energy required to split up the defects cluster into well separated non-interacting defects were calculated using the method proposed by Zollo *et al* [47]. For the V_{Ge}-Tm_i^{3+} in the axial configuration, we obtained a binding energy of 4.21 for the neutral state, showing the stability of the V_{Ge}-Tm_i^{3+} defect.

3. Results and Discussion

3.1. Structural Properties and Energetics of Tm^{3+} defects in Ge

The relaxed geometric structures of Tm^{3+} defects in Ge are shown in Fig. 1. Fig. 1a represent the structure of the Tm_i^{3+} in the H configuration. In this configuration, the angle between the defect atom and the nearest Ge atom before and after relaxation was 86^0 and 94^0 respectively. The interstitial atom caused a change in atomic position after relaxation which led to a bond length reduction between the Tm and Ge atoms by 0.05 Å. The geometric structures of the V_{Ge}-Tm_i^{3+} in both the *axial* and *basal* configurations are displayed in Fig. 1b and Fig. 1c, respectively. In both configurations, after

relaxation, the bond lengths between the defect atom and its two nearest Ge neighbours were reduced from 2.88 to 2.71 Å and from 3.02 to 2.92 Å. For the V_{Ge}-Tm_i^{3+} , the bond angle between the Tm atom and two nearest Ge neighbours was reduced from 52.7^0 to 51.3^0. It was interesting to note that the same change of bond length and bond angle was observed in both the *axial* and *basal* configurations except that the position of the vacancy atom differed. The geometric structure of the Tm_{Ge}^{3+} is shown in Figure 1d. The introduction of the substitutional defect led to structural rearrangement of the Ge crystal supercell. After the relaxation of the Tm_{Ge}^{3+}, the bond length and bond angle which it forms with the nearest Ge atoms reduced by 0.01 Å and 0.9^0 respectively.

3.2. Properties and Energetics of Tm_i^{3+}

The energy of formation (E^f) for the positive, neutral and negative charge states of Tm_i^{3+}, V_{Ge}-Tm_i^{3+} and Tm_{Ge}^{3+} are presented in Table 1. For the Tm_i^{3+} in the hexagonal (H) configuration, the formation energies varied from 4.35 to 1.96 eV. The E^f decreased from the double negative to the double positive charge states. The formation energies of the defects in their charged states were low, and the charge state +2 had the lowest formation energy at $\varepsilon_F = 0$. The low formation energies of Tm_i^{3+} in the H configuration for all the charge states suggested that under equilibrium conditions, Tm_i^{3+} can form relatively easily. It should be noted that, even though the formation energies for Tm_i^{3+} in the H configuration were low, the Tm_i^{3+} was more energetically favourable (in all charge states) in the tetrahedral (T) configuration [48] see Table 1. The formation energies of Tm_i^{3+} in its charge states as a function of ε_F are shown in Fig. 2b. The Tm_i^{3+} defect introduced transition state levels in the band

gap that were either single acceptor or double donor. The energy level of the acceptor state related to the valence band maximum (VBM) was $\epsilon(0/-1)$ = 0.65 eV and the other transition levels were $\epsilon(+1/0) = 0.55$ eV and $\epsilon(+1/+2)$ = 0.22 eV above the VBM for the single and double donors respectively. The -1, 0, $+1$, and $+2$ charge states were thermodynamically accessible. Charge state -2 was not thermodynamically stable for any Fermi-level in the band gap. The difference in energy level between $\epsilon(+1/0)$ and $\epsilon(0/-1)$ was 0.10 eV. The H configuration, although not the most energetically stable configuration of Tm_i^{3+} displayed some transition levels as reported above that were not found in the T configuration. The T configuration exhibited only the properties of shallow double donor level at $E_C - 0.04$ eV [48] see Table 2a. The interaction energy between two electrons in a two-level defect is referred to as Hubbard U. Fig. 2b shows that the Tm_i^{3+} impurity has a *positive*$-U$ property with small *effective-* U value of 0.09 eV.

3.3. Properties and Energetics of V_{Ge}-Tm_i^{3+}

In this defect, we have two major configurations namely: the *axial* and *basal* configurations derived from the position of the vacancy atom, see Fig. 1b and Fig. 1c. In Table 1, we show that the formation energies of V_{Ge}-Tm_i^{3+} for charge states -2 to $+2$ varied from 0.84 to 2.55 eV and from 5.04 to 6.93 for the *axial* and *basal* configurations respectively. In both configurations, the E^f decreased from the double negative to the double positive charge states. The formation energies of the charged states were relatively low. In both configurations, the $+2$ charge state had the lowest formation energy at $\varepsilon_F = 0$ compared to other charge states. The *axial* configuration has lower formation energies than the *basal* configuration in all the charge

states. The low formation energies indicate that the V_{Ge}-Tm_i^{3+} defect can form easily in the two different configurations. It is interesting to know that the formation energies of the V_{Ge}-Tm_i^{3+} in the *axial* configuration were lower than that of the Tm_i^{3+} in the H configuration, while for the Tm_i^{3+} in the H configuration, the formation energies for all the charge states were lower than that of the *basal* configuration of the V_{Ge}-Tm_i^{3+}. The plot of the formation energies of V_{Ge}-Tm_i^{3+} in its charge states as a function of ε_F are shown in Fig. 2c and Fig. 2d for both the *axial* and *basal* configurations respectively. For both configurations, the defect introduced both acceptor and donor levels that were deep lying within the band gap. For the *axial* configuration, double $\epsilon(-1/-2)$ and single $\epsilon(0/-1)$ acceptor levels were found lying close to the CBM and close to the middle of the band gap respectively. This same trend was also observed for the *basal* configuration. While the $\epsilon(-1/-2)$ transition level for the *axial* configuration was 0.10 eV away from the CBM, for the *basal* configuration it was 0.14 eV away from the CBM. V_{Ge}-Tm_i^{3+} also introduced other transition states, single $\epsilon(+1/0)$ and double $\epsilon(+1/+2)$ donor levels in the band gap. As was observed for the acceptor levels, the donor levels were close to the band edges. For the $\epsilon(+1/0)$ level, it was near the middle of the band gap for both configurations. While the $\epsilon(+2/+1)$ for the *axial* configuration was 0.19 eV away from the VBM, for the *basal* configuration, it was 0.27 eV away from the VBM. In both configurations, all the charge states (+2 to -2) were thermodynamically accessible and stable for some values of the Fermi-level, but this was not the case for the Tm_i^{3+} were we found that the defect was never stable in the negative 2 charge state. As was observed in the Tm_i^{3+}, both the *axial* and *basal* configura-

tions displayed *positive*$-U$ behaviour with small *effective*$-U$ values of 0.23 and 0.10 eV respectively.

3.4. Properties and Energetics of Tm^{3+}_{Ge}

The formation energies of the positive, neutral and negative charge states of Tm^{3+}_{Ge}, as shown in Table 1, show a decrease from the double negative to the double positive charge states. The formation energies varied from 1.83 to 3.37 eV. The formation energy of the Tm^{3+}_{Ge} is relatively low, although higher than that of the V_{Ge}-Tm^{3+}_{i} for the *axial* configuration, and lower than the formation energies of both the Tm^{3+}_{i} in the H configuration and V_{Ge}-Tm^{3+}_{i} in the (*basal* configuration) in all the charge states. In this present work, the sequence of formation energy from high to low was V_{Ge}-Tm^{3+}_{i} (*basal*)>Tm^{3+}_{i} >Tm^{3+}_{Ge} >V_{Ge}-Tm^{3+}_{i} (*axial*). In our results, the Tm^{3+}_{Ge} substitutional defect was energetically more favourable than the interstitial in the H configuration, but the T configuration was energetically much more favourable than the Tm^{3+}_{Ge} as was discussed in our earlier work [48]. The plot of the the formation energy of Tm^{3+}_{Ge} in its charge states as a function of ε_F is shown in Fig. 2e. The defect introduced a double acceptor level at $\epsilon(-1/-2)$, lying close to the edge of the band gap (CBM) at $E_C - 0.05$ eV. The donor levels induced by Tm^{3+}_{Ge} in the band gap were a double donor at $E_V + 0.10$ and a single donor at $E_V + 0.19$ eV. The Tm^{3+}_{Ge} defect in Ge also induced a $\epsilon(0/-1)$ transition level lying at the middle of the band gap. The Tm^{3+}_{Ge} displayed *positive*$-U$ behaviour with a small *effective*$-U$ value of 0.32 eV. We show that not only Tm^{3+}_{i} interstitial defects in Ge occur at a low formation energy in all the charge states but that this also applies to the V_{Ge}-Tm^{3+}_{i} and Tm^{3+}_{Ge} defects.

4. Summary

We have carried out detailed calculations of Tm^{3+} (interstitial, vacancy-complex and substitution) related defects in Ge, using a hybrid functional (HSE06) in the framework of density functional theory (DFT). The formation energies and thermodynamic charge transition levels were described in detail. We have shown that the formation of Tm_i^{3+} in the hexagonal configuration, Tm_{Ge}^{3+}, and V_{Ge}-Tm_i^{3+} for two configurations (*axial and basal*) defects in Ge exist with low formation energies. Our calculation shows that V_{Ge}-Tm_i^{3+} in the *axial* configuration had the lowest formation energy for the neutral, negative and the positive charge states. We have shown also that Tm_{Ge}^{3+} forms with a lower formation energy than the Tm_i^{3+} for the H configurations. In addition to the low formation energies, we have shown that Tm_i^{3+}, Tm_{Ge}^{3+}, and V_{Ge}-Tm_i^{3+} defect introduced transition levels of $(0/-1)$ and $(+1/0)$ that were lying deep in the band gap. The V_{Ge}-Tm_i^{3+} and Tm_{Ge}^{3+} introduced additional $(+1/+2)$ and $(-1/-2)$ levels that were lying close to the band edges. Unlike the Tm_{Ge}^{3+} and V_{Ge}-Tm_i^{3+} that acts as a double acceptor $(-1/-2)$, the Tm_i^{3+} does not act as a double acceptor instead, this level lies inside the CBM. We expect the data and information presented to be useful in the process modelling of Ge-based devices.

5. Acknowledgement

This work is based on the research supported partly by National Research foundation (NRF) of South Africa (Grant specific unique reference number (UID) 78838). The opinions, findings and conclusion expressed are those of

the authors and the NRF accepts no liability whatsoever in this regard. The authors also acknowledged MedeA VASP.

[1] L. Lee, E. A. Fitzgerald, T. Bulsara, Mayank, T. Currie, A. Lochtefeld, Journal of Applied Physics 97 (1) (2005) 011101.

[2] H. Tahini, A. Chroneos, R. W. Grimes, U. Schwingenschlgl, A. Dimoulas, Journal of Physics: Condensed Matter 24 (19) (2012) 195802.

[3] M. Houssa, A. Satta, E. Simoen, B. De, M. Jaeger, M. Caymax, M. Heyns, Germanium-Based Technologies: From Materials to Devices (2011) 233.

[4] A. Chroneos, H. Bracht, Applied Physics Reviews 1 (1) 011301.

[5] J. Coutinho, R. Jones, P. R. Briddon, S. Öberg, Phys. Rev. B 62 (2000) 10824–10840.

[6] E. Igumbor, C. Ouma, G. Webb, W. Meyer, Physica B: Condensed Matter 480 (2016) 191 – 195.

[7] C. Nyamhere, M. Das, F. D. Auret, A. Chawanda, physica status solidi (c) 5 (2) (2008) 623–625.

[8] F. Auret, P. J. van Rensburg, M. Hayes, J. Nel, S. Coelho, W. Meyer, S. Decoster, V. Matias, A. Vantomme, D. Smeets, Nuclear Instruments and Methods in Physics Research Section B: Beam Interactions with Materials and Atoms 257 (12) (2007) 169 – 171.

[9] J. Fage-Pedersen, A. N. Larsen, A. Mesli, Phys. Rev. B 62 (2000) 10116–10125.

[10] H. Haesslein, R. Sielemann, C. Zistl, Phys. Rev. Lett. 80 (1998) 2626–2629.

[11] R. Sielemann, Nuclear Instruments and Methods in Physics Research 146 (14) (1998) 329 – 340.

[12] C. Claeys, E. Simoen, Germanium-based technologies: from materials to devices, Elsevier, 2011.

[13] M. Lourenço, C. Opoku, R. Gwilliam, K. Homewood, Optical Materials 32 (12) (2010) 1597–1600.

[14] A. Polman, Journal of Applied Physics 82 (1) (1997) 1–39.

[15] M. A. Loureno, R. M. Gwilliam, K. P. Homewood, Applied Physics Letters 92 (16).

[16] F. Fang, A. Ng, X. Chen, A. Djurii, Y. Zhong, K. Wong, P. Fong, H. Lui, C. Surya, W. Chan, Materials Chemistry and Physics 125 (3) (2011) 813 – 817.

[17] L. C. Courrol, I. M. Ranieri, S. L. Baldochi, R. E. Samad, A. Z. de Freitas, L. Gomes, N. D. Vieira, Optics communications 270 (2) (2007) 340–346.

[18] R. Paschotta, P. R. Barber, A. C. Tropper, D. C. Hanna, J. Opt. Soc. Am. B 14 (5) (1997) 1213–1218.

[19] T. Monteiro, A. J. Neves, M. J. Soares, M. C. Carmo, M. Peres, E. Alves, E. Rita, Applied Physics Letters 87 (19) (2005) –.

[20] W. Jadwisienczak, H. Lozykowski, A. Xu, B. Patel, Visible emission from ZnO doped with rare-earth ions, Journal of Electronic Materials 31 (7) (2002) 776–784.

[21] E. Rita, E. Alves, U. Wahl, J. Correia, A. Neves, M. Soares, T. Monteiro, Physica B: Condensed Matter 340342 (0) (2003) 235 – 239.

[22] T. Andreev, N. Q. Liem, Y. Hori, M. Tanaka, O. Oda, D. L. S. Dang, B. Daudin, B. Gayral, Phys. Rev. B 74 (2006) 155310.

[23] M. Peres, J. Wang, M. Soares, A. Neves, T. Monteiro, E. Rita, U. Wahl, J. Correia, E. Alves, Superlattices and Microstructures 36 (46) (2004) 747 – 753.

[24] G. S. Pomrenke, E. Silkowski, J. E. Colon, D. J. Topp, Y. K. Yeo, R. L. Hengehold, Journal of Applied Physics 71 (4).

[25] H. Przybylinska, W. Jantsch, Y. Suprun-Belevitch, M. Stepikhova, L. Palmetshofer, G. Hendorfer, A. Kozanecki, R. J. Wilson, B. J. Sealy, Phys. Rev. B 54 (1996) 2532–2547.

[26] Y. Miyata, Y. Nose, T. Yoshimura, A. Ashida, N. Fujimura, Journal of Crystal Growth 425 (2015) 158 – 161.

[27] J. Heyd, G. E. Scuseria, M. Ernzerhof, The Journal of Chemical Physics 118 (18) (2003) 8207–8215.

[28] G. Kresse, J. Furthmüller, Phys. Rev. B 54 (1996) 11169–11186.

[29] G. Kresse, D. Joubert, Phys. Rev. B 59 (1999) 1758–1775.

[30] P. E. Blochl, Phys. Rev. B 50 (1994) 17953–17979.

[31] J. P. Perdew, K. Burke, M. Ernzerhof, Phys. Rev. Lett. 77 (1996) 3865–3868.

[32] H. Tahini, A. Chroneos, R. W. Grimes, U. Schwingenschlgl, H. Bracht, Applied Physics Letters 99 (7) 072112.

[33] P. Śpiewak, J. Vanhellemont, K. Sueoka, K. Kurzydłowski, I. Romandic, Materials Science in Semiconductor Processing 11 (5) (2008) 328–331.

[34] P. Deák, B. Aradi, T. Frauenheim, E. Janzén, A. Gali, Phys. Rev. B 81 (2010) 153203.

[35] B. G. Janesko, T. M. Henderson, G. E. Scuseria, Physical Chemistry Chemical Physics 11 (3) (2009) 443–454.

[36] V. I. Anisimov, J. Zaanen, O. K. Andersen, Physical Review B 44 (3) (1991) 943.

[37] L. Petit, A. Svane, Z. Szotek, W. M. Temmerman, Physical Review B 72 (20) (2005) 205118.

[38] M. Cococcioni, S. De Gironcoli, Physical Review B 71 (3) (2005) 035105.

[39] J. L. Da Silva, M. V. Ganduglia-Pirovano, J. Sauer, V. Bayer, G. Kresse, Physical Review B 75 (4) (2007) 045121.

[40] H. J. Monkhorst, J. D. Pack, Phys. Rev. B 13 (1976) 5188–5192.

[41] S. B. Zhang, J. E. Northrup, Phys. Rev. Lett. 67 (1991) 2339–2342.

[42] Freysoldt, Christoph, Grabowski, Blazej, Hickel, Tilmann, J. Neugebauer, Kresse, Georg, Janotti, Anderson, V. de Walle, C. G., Rev. Mod. Phys. 86 (2014) 253–305.

[43] Y. Kumagai, F. Oba, Phys. Rev. B 89 (2014) 195205.

[44] S. Lany, A. Zunger, Physical Review B 78 (23) (2008) 235104.

[45] J. P. Perdew, M. Levy, Phys. Rev. Lett. 51 (1983) 1884–1887.

[46] F. J. Morin, J. P. Maita, Phys. Rev. 94 (1954) 1525–1529.

[47] G. Zollo, Y. J. Lee, R. M. Nieminen, Journal of Physics: Condensed Matter 16 (49) (2004) 8991.

[48] E. Igumbor, W. E. Meyer, conference proceeding of the 60th Annual Conference of the South African Institute of Physics submitted to SAIP Journal. Phys (2015).

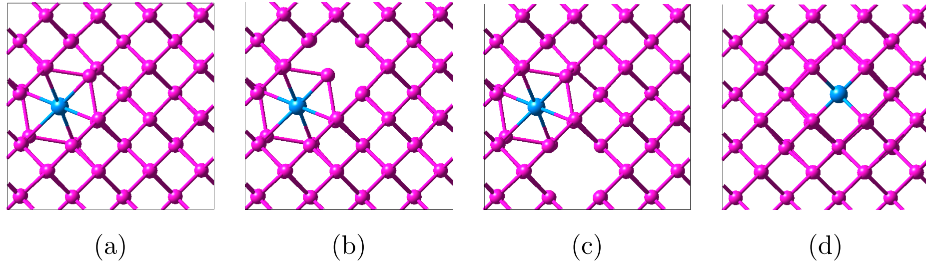

(a) (b) (c) (d)

Figure 1: The relaxed structures of Tm^{3+} defects in Ge, defect atom in blue and the wide space in the crystal structure indicating the position of the Ge vacancy; (a) H configuration of Tm_i^{3+}, (b) V_{Ge}-Tm_i^{3+} *(axial)* (c) V_{Ge}-Tm_i^{3+} *(basal)* and (d) Tm_{Ge}^{3+}.

Table 1: Calculated formation energies (E^f) in eV at $\epsilon_f = 0$ of Tm^{3+} interstitial (Tm_i^{3+}), substitutional (Tm_{Ge}^{3+}) and vacancy-interstitial complex (V_{Ge}-Tm_i^{3+}) in Ge. The result of the Tm_i^{3+} tetrahedral configuration was from Ref [48].

Defect	Configuration	-2	-1	0	$+1$	$+2$
Tm_i^{3+}	*tetrahedral*	3.94	2.75	1.81	0.89	0.24
	hexagonal	4.35	3.37	2.73	2.18	1.96
V_{Ge}-Tm_i^{3+}	*axial*	2.55	1.87	1.39	1.04	0.84
	basal	6.93	6.29	5.75	5.31	5.04
Tm_{Ge}^{3+}		3.37	2.64	2.12	1.92	1.83

Table 2: The energy of the thermodynamic transition levels $\epsilon(q/q')$ above E_V (eV) for the Tm^{3+} interstitial, substitution and vacancy-interstitial complex in Ge.

Charge States	Tm_i^{3+} (T)	Tm_i^{3+} (H)	$V_{Ge}-Tm_i^{3+}$(*basal*)	V_{Ge}-Tm_i^{3+} (*axial*)	Tm_{Ge}^{3+}
$(-1/-2)$	-	-	0.64	0.68	0.73
$(0/-1)$	-	0.65	0.55	0.48	0.52
$(+1/0)$	-	0.55	0.44	0.34	0.19
$(+2/+1)$	0.74 [48]	0.22	0.27	0.19	0.10

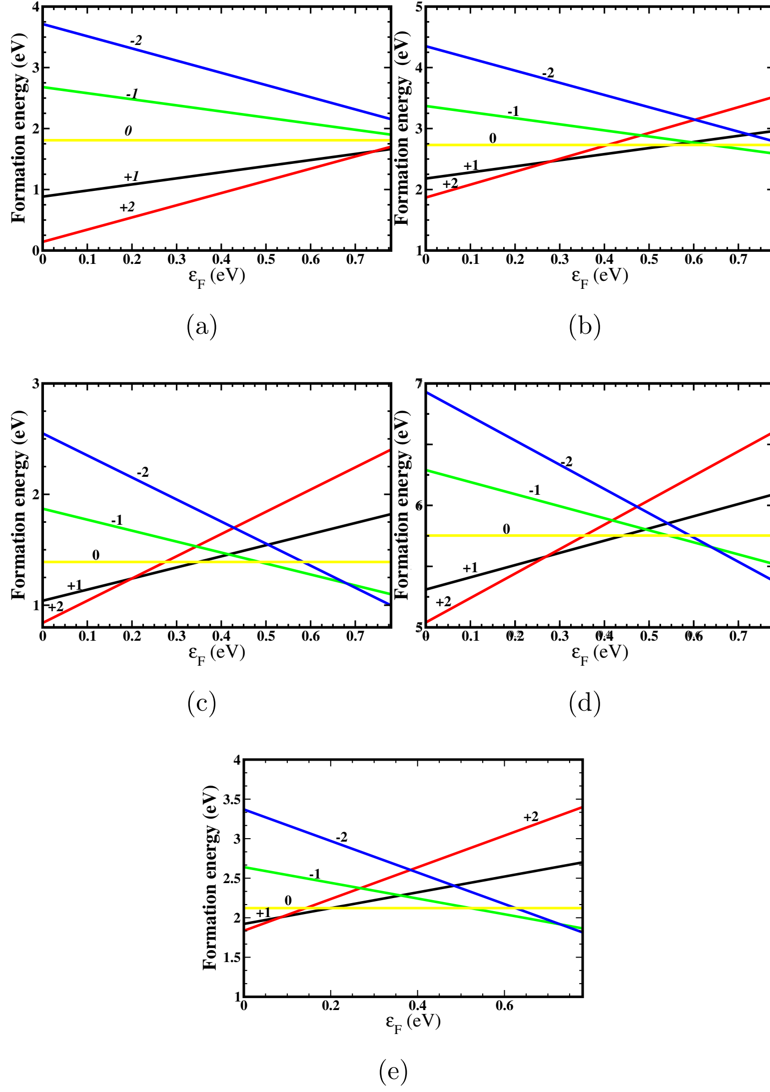

Figure 2: Plot of formation energy as a function of the Fermi energy for the Tm_i^{3+}, V_{Ge}-$Tm_i{}^{3+}$ (*axial and basal*) and substitution Tm_{Ge}^{3+} in Ge; (a) *tetrahedral* configuration of Tm_i^{3+}, (b) *hexagonal* configuration of Tm_i^{3+}, (c) V_{Ge}-$Tm_i{}^{3+}$ configuration (*axial*), (d) V_{Ge}-$Tm_i{}^{3+}$ configuration (*basal*) and (e) Tm_{Ge}^{3+}.